Design of RST and Fractional order PID controllers for an Induction motor drive for Electric Vehicle Application

M Bendjedia, K A Tehrani, Y Azzouz

Embedded Electronic Systems Research Institute (IRSEEM), Ecole Supérieure d'Ingénieurs en Génie Electriques (ESIGELEC)
Technopôle du Madrillet, Saint-Etienne du Rouvray 76800, France.
Moussa.bendjedia@esigelec.fr, kambiz.tehrani@esigelec.fr, yacine.azzouz@esigelec.fr.

Keywords: Induction motor drive, RST controller, Fractional order PID controller, indirect stator-flux-oriented control (ISFOC).

Abstract

This paper aims to provide a new robust control system for an induction motor used in electric vehicle (EV). The speed control is based on a polynomial RST controller which can reject disturbance with no steady state errors. High-dynamic performance is obtained using the indirect stator-flux-oriented control (ISFOC) and the space vector pulse width modulation (SVPWM) techniques. For current regulation, we proposed a new fractional order proportional-integral-derivative (FOPID) controller based on the multi-objective optimisation evolutionary algorithm (EA). Therefore an excellent start-up response is obtained furthermore the desired dynamic response without unexpected switching behaviour. The proposed control strategies have been simulated on a 3-kW induction-motor drive for an EV. Simulation results show the robustness and effectiveness of the proposed approaches.

1 Introduction

With the requirements for reducing emissions and improving fuel economy, automotive companies are developing electric (EV), hybrid electric (HEV), and plug-in hybrid electric vehicles (PHEV) [1]. This work is part of a research project concerning the development of a new extended range of urban electric vehicle based multi-source system. The new electrical vehicle run slowly on electricity until the battery needs to be recharged. The gasoline engine will then generate the electricity needed to charge the batteries which can also charged by solar panels.

The main requirements of the EV drive are high efficiency over wide speed and torque range, fast torque response and robustness for various operating conditions. The induction motors are widely used for electric propulsion because they are characterized by reliability ruggedness, low maintenance, low cost, and ability to operate in hostile environments [2]. The proportional-integral-derivative (PID) controller has been widely used in industry applications such as motor control because it has simple structure with easy parameters tuning. However, this conventional controller is no longer satisfying the operating conditions requirements of the EV. Therefore, advanced regulators must be used in order to fulfill these requirements.

The RST controller is an efficient strategy of digital control and it has been used in many applications. For HEV, it has been applied to DC/DC converter to ensure energy management between supercapacitor and battery [3,4]. The RST controller is designed for battery charger of the EV [5]. The RST controller is also used in power energy systems [6] and it has shown a good performance, in terms of rapidity, tracking and robustness. In [7], this controller has been proposed to control the rotor position of the hybrid step motor where a high accuracy of positioning is required.

The performance of conventional PID controllers can be improved by using fractional order derivatives and integrals. The FOPID was proposed first time by Podlubny [8,9] and subsequently, it has received a great attention by researchers [10-11]. The FOPID controller is more flexible and can provide an opportunity to better adjust the dynamical characteristics of the control system. FOPID design is also a parameter optimization problem. Design of FOPID controllers can be considered as a real parameter optimization problem in a five-dimensional hyperspace. We found the five parameters that can be done through optimization design of an FOPID controller by a genetic algorithm. The optimization of the parameters of a FOPID is much more difficult than conventional PID. Several methods have been proposed for this design by using optimization methods [10-16].

In this paper, we propose a robust control system for an induction motor used in electric vehicle (EV). We designed an advanced RST controller for speed control and a new robust current control system by FOPID controller. In order to obtain better hhigh-dynamic performance; we used the ISFOC and the SVPWM techniques. The Strength Pareto Evolutionary Algorithm is used as a multi-objective optimization approach for the design of this controller. The results show excellent performance of the control system.

This paper is organized as follow. Section 2 shows the stator flux orientation control; section 3 presents the procedure design of the RST controller. Then, the design of the FOPID controller is explained in section 4. The corresponding simulation results are presented in section 5.

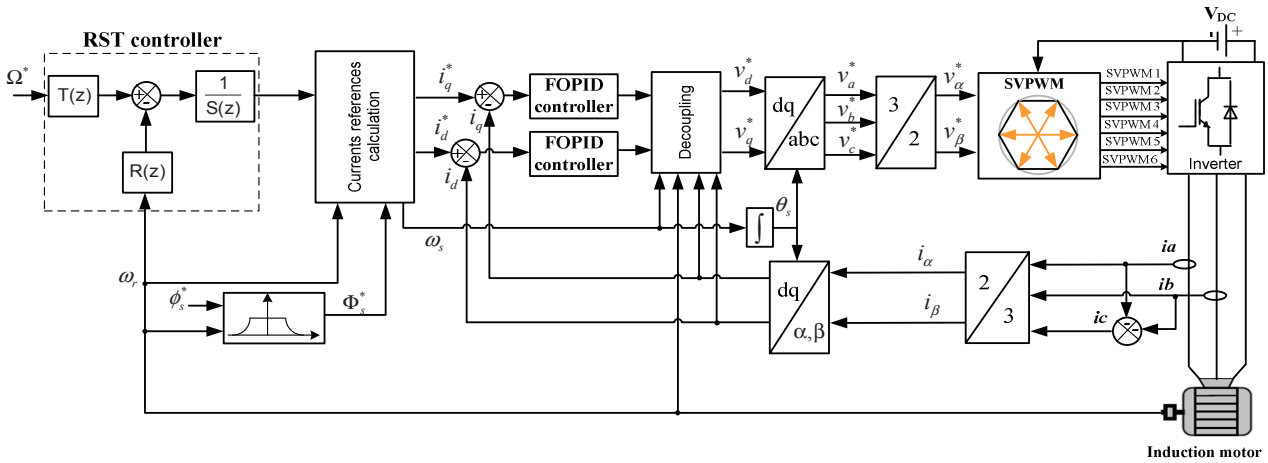

Fig. 1: Block diagram of the proposed control of induction motor

2 Stator flux orientation control

The dynamic model of the induction motor expressed in the *d-q* axis reference frame is given as follows [17].

$$\begin{cases} \frac{d\Phi_{ds}}{dt} = \omega_s \Phi_{qs} - R_s i_{ds} + v_{ds} \\ \frac{d\Phi_{qs}}{dt} = -\omega_s \Phi_{ds} - R_s i_{qs} + v_{qs} \\ \frac{di_{ds}}{dt} = \frac{1}{\sigma\tau_r L_s}\Phi_{ds} + \frac{\omega_r}{\sigma L_s}\Phi_{qs} - \frac{(\tau_s+\tau_r)1}{\sigma\tau_s\tau_r} i_{ds} + \omega_{sl} i_{qs} + \frac{1}{\sigma L_s} v_{ds} \\ \frac{di_{qs}}{dt} = -\frac{\omega_r}{\sigma L_s}\Phi_{ds} + \frac{1}{\sigma\tau_r L_s}\Phi_{qs} - \omega_{sl} i_{ds} - \frac{(\tau_s+\tau_r)1}{\sigma\tau_s\tau_r} i_{qs} + \frac{1}{\sigma L_s} v_{qs} \\ \frac{d\omega_r}{dt} = \frac{N_p^2}{J} i_{qs}\Phi_{ds} - \frac{N_p^2}{J} i_{ds}\Phi_{qs} - \frac{f}{J}\omega_r - \frac{N_p}{J} T_L \end{cases} \quad (1)$$

Where $\omega_{sl} = \omega_s - \omega_r$, $\tau_r = \frac{L_r}{R_r}$, $\tau_s = \frac{L_s}{R_s}$, and $\sigma = 1 - \frac{M^2}{L_s L_r}$

For stator flux orientation, the rated flux is aligned along the *d*-axis, therefore $\Phi_{ds} = \Phi_s$ and $\Phi_{qs} = 0$.

The torque is controlled by using the *q*-axis current as follows.

$$T_e = N_p \Phi_{ds} i_{qs} \quad (3)$$

The *d* and *q*-axis command stator voltage are given by

$$\begin{aligned} v_{ds} &= \sigma L_s \left(p + \frac{\tau_s+\tau_r}{\sigma\tau_s\tau_r} \right) i_{ds}^* - \frac{1}{\tau_r}\phi_s^* - \sigma L_s \omega_{sl}^* i_{qs}^* \\ v_{qs} &= \sigma L_s \left(p + \frac{\tau_s+\tau_r}{\sigma\tau_s\tau_r} \right) i_{qs}^* + \frac{\omega_r}{\tau_r}\phi_s^* + \sigma L_s \omega_{sl}^* i_{ds}^* \end{aligned} \quad (4)$$

As shown in (4), the stator voltage components are coupled by the *d*- and *q*- back electromotive force given by

$$\begin{aligned} v_d^{dec} &= -\frac{1}{\tau_r}\phi_s^* - \sigma L_s \omega_{sl}^* i_{qs}^* \\ v_d^{dec} &= \frac{\omega_r}{\tau_r}\phi_s^* + \sigma L_s \omega_{sl}^* i_{ds}^* \end{aligned} \quad (5)$$

The *d*-axis voltage depends on *q*-axis current, and *q*-axis voltage depends also on *d*-axis current. The feedforward decoupling method [18] is applied in order to have linear terms as follows

$$\begin{aligned} v_d &= v_{ds} - v_{ds}^{dec} = \sigma L_s \left(p + \frac{\tau_s+\tau_r}{\sigma\tau_s\tau_r} \right) i_{ds}^* \\ v_q &= v_{ds} - v_{qs}^{dec} = \sigma L_s \left(p + \frac{\tau_s+\tau_r}{\sigma\tau_s\tau_r} \right) i_{qs}^* \end{aligned} \quad (6)$$

The proposed control of the induction motor is presented in Fig. 1. The SVPWM is more sophisticated technique to provide a higher voltage to the induction motor compared with a classical sine pulse width modulation (SPWM). The basis of SVPWM is different from that of SPWM [19]. SPWM aims to achieve symmetrical 3-phase sine voltage waveforms of adjustable voltage and frequency, while the SVPWM uses the eight fundamental voltage vectors to realize variable frequency of voltage and speed adjustment and it offers better DC bus utilization.

3 RST controller design

The RST controller consists of the following functional diagram with three branches:

Fig. 2: Block Diagram of RST Controller

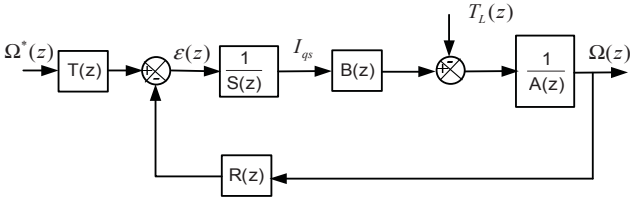

The synthesis of the RST controller consists to find the parameters of the polynomials *S(z)*, *R(z)* and *T(z)* in order to achieve the desired performances of the closed loop system.
The motor transfer function in continuous domain is given by:

$$F(p)=\frac{K}{p+p_1} \tag{7}$$

Where $K=\frac{N_p\Phi_s}{J}$ and $p_1=\frac{f}{J}$

By using a zero order hold (ZOH) the discrete model of *F(p)* is given by

$$H(z)=\frac{B(z)}{A(z)}=\frac{K_1(1-z_1)z^{-1}}{1-z_1z^{-1}}=\frac{b_0+b_1z^{-1}}{a_0+a_1z^{-1}} \tag{8}$$

where

$$K_1=\frac{K}{p_1},\ z_1=e^{-p_1T},\ b_0=0,\ b_1=K_1(1-z_1),\ a_0=1,\ a_1=-z_1$$

The output speed can be expressed as follows (see Fig. 2):

$$\Omega=\frac{T(z)B(z)}{A(z)S(z)+B(z)R(z)}\Omega^*-\frac{A(z)S(z)}{A(z)S(z)+B(z)R(z)}T_L \tag{9}$$

The load torque T_L is considered just as disturbance.
The simplest method for the synthesis of the RST controller consists in finding the polynomials *R(z)* and *S(z)* which appear in the denominator of (9) by imposing the root locus of the characteristic equation (i.e., the poles in closed loop system), in order to achieve desired performances. Let's denote the characteristic polynomial of the closed loop system by *P(z)*. Since *A(z)* and *B(z)* are known from (8), we have to solve the following equation to determine the polynomials *R(z)* and *S(z)*:

$$P(z)=A(z)R(z)+B(z)S(z) \tag{10}$$

For polynomial *T(z)*, we can take a constant which ensures a unit static gain between $\Omega^*(z)$ and $\Omega(z)$. A strictly proper controller is used, therefore the degrees of the polynomials *P(z)*, *R(z)* and *S(z)* are given by

$$\begin{aligned}&\deg(P(z))=2\deg(A(z))+1=3\\&\deg(S(z))=\deg(A(z))+1=2\\&\deg(R(z))=\deg(A(z))=1\end{aligned} \tag{11}$$

So, the polynomials *P(z)*, *R(z)* and *S(z)* can be written as:

$$P(z)=1+p_1z^{-1}+p_2z^{-2}+p_3z^{-3} \tag{12}$$

$$S(z)=(1-z^{-1})(s_0+s_1z^{-1}) \tag{13}$$

$$R(z)=r_0+r_1z^{-1}) \tag{14}$$

In (13), an integration action is introduced in *S(z)* in order to ensure a load torque disturbance rejection.
The coefficients of *S(z)* and *R(z)* are obtained by imposing three poles for the closed loop . We choose a pair of complex conjugate poles that the imaginary part is equal to the negative real part and the third pole also is equal to the negative real part as follow:

$$p_{1,2}=-\zeta\omega_0\pm j\zeta\omega_0 \text{ and } p_3=-\zeta\omega_0 \tag{15}$$

To get the real part equal to the imaginary part, it is necessary to take $\zeta = 0.707$. In this case, the overshoot created by the pair of the complex conjugate poles is compensated by the real pole.
The polynomial *P(z)* that contains the poles can be written in the discrete domain as follows:

$$P(z)=(1+a_{d1}z^{-1}+a_{d2}z^{-2})(1+z_3z^{-1}) \tag{16}$$

with $a_{d1}=-2e^{-\zeta\omega_0T}\cos(\omega_aT)$; $a_{d1}=e^{-2\zeta\omega_0T}$; $z_3=-e^{-\zeta\omega_0T}$
The equation (10) becomes:

$$\begin{aligned}P(z)=&\left(a_0+a_1z^{-1}\right)\left(1-z^{-1}\right)\left(s_0+s_1z^{-1}\right)\\&+\left(b_0+b_1z^{-1}\right)\left(r_0+r_1z^{-1}\right)\end{aligned} \tag{17}$$

The identification between (16) and (17) makes it possible to find the coefficients of the two polynomials *R(z)* and *S(z)*.
The polynomial *T(z)*, can be a constant that guarantee null steady-state error. By using (9) and considering that *S(z)* is null in steady state, *T(z)* can be obtained as follows

$$T(z)=r_0+r_1 \tag{18}$$

4 FOPID controller design

Fractional calculus is a branch of mathematics dealing with real number powers of differential or integral operators. It generalizes the common concepts of derivative and integral. The most usual definition of fractional calculus has been proposed in [11] as follows:

$${}_cD_x^{-n}f(x)=\int_c^x\frac{(x-t)^{n-1}}{(x-t)!}f(t)dt,\quad n\in\Re \tag{19}$$

The general definition of D is given by (2):

$${}_cD_x^{v}f(x)=\begin{cases}\int_c^x\frac{(x-t)^{-v-1}}{\Gamma(-v)}f(t)dt, & if\ v<0\\ f(t), & if\ v=0\\ D^n\left[{}_cD_x^{v-n}f(x)\right], & if\ v>0\end{cases} \tag{20}$$

$n=\min\{K\in\Re,\ K>v\}$
$\Gamma(\cdot)$ is the Euler's gamma function.

The approximation of fractional order derivative and integral is based on the Crone approach.
The functions we are dealing with provide integer-order frequency-domain approximation of transfer functions involving fractional powers of s. For the frequency-domain transfer function C(s) which is given by :

$$C(s) = Ks^{v} \qquad v \in \Re \tag{21}$$

This approximation implements a recursive distribution of N zeros and N poles leading to a transfer function as follows.

$$C(s) = K' \prod_{n=1}^{N} \frac{1 + \frac{s}{\omega_{zn}}}{1 + \frac{s}{\omega_{pn}}} \tag{22}$$

Where K' is an adjusted gain so that both (21) and (22) have unit gain at 1 rad/s. Zeros and poles have to be found over a frequency domain $[\omega_l; \omega_h]$ where the approximation is valid, they are given, for a positive v, by :

$$\omega_{z1} = \omega_l \sqrt{\eta} \tag{23}$$

$$\omega_{pn} = \omega_{z,n-1} \alpha \qquad n = 1...N \tag{24}$$

$$\omega_{zn} = \omega_{p,n-1} \eta \qquad n = 1...N \tag{25}$$

Where $\alpha = \left(\frac{\omega_h}{\omega_l} \right)^{\frac{v}{N}}$ and $\eta = \left(\frac{\omega_h}{\omega_l} \right)^{\frac{1-v}{N}}$

For negative values of v, the role of the zeros and the poles is swapped. The number of poles and zeros is selected at first and the desired performance of this approximation depends on the order N. Simple approximation can be provided with lower order N, but it can cause ripples in both gain and phase characteristics. When $|v|>1$, the approximation is not satisfactory. The fractional order v usually is separated as in (26) and only the first term s^{β} needs to be approximated.

$$s^{v} = s^{\beta} s^{n}, \quad v = n + \beta, \; n \in \Re, \; \beta \in [0,1] \tag{26}$$

The general form of fractional order PID controller is $PI^{\alpha}D^{\beta}$ and its general transfer function is given by

$$G_c(s) = K_p + K_I S^{-\alpha} + K_D S^{\beta} \tag{27}$$

Besides selecting K_p, K_I, and K_D, it needs to select α and β which are not necessarily integer numbers.

The calculation of these five parameters can be done through optimization. Since the design of FOPID can be considered as a parameter-optimization problem and the features of the system are conflicting, we used a Multi-Objective optimization method called strength pareto evolutionary algorithm (SPEA) for this problem. This SPEA integrates established techniques used in existing evolutionary algorithms (EA's) in a single algorithm and its convergence to pareto optimal front (POF) is an advantage over other EA's. The SPEA is based on the following steps:

SPEA Algorithm [15]:

1) Produces a random parent population P and form the empty external non-dominated set P'.
2) Pastes non-dominated members of P into P'.
3) Eliminates all solutions within P' which are covered by any other members of P'.
4) If the number of externally stored non-dominated solutions exceeds a given maximum N', uses clustering to prune P'.
5) Assigns fitness to all individuals in P and P'.
6) Selects individuals from P and P' using binary tournament selection with replacement until the mating pool is filled.
7) Applies genetic operators (crossover and mutation) as usual.
8) If the maximum number of generations is reached, then stop, else go to step 2.

5 Simulation results

This section presents the simulation results obtained from speed control of the induction motor drives as shown in Fig. 1. The simulation was performed with Matlab/Simulink software environment. The proposed control strategies have been simulated on a 3-kW induction-motor drive whose parameters are listed in Table I.

Specifications		*Parameters*	
Rated power	3kW	R_s	2.3 Ω
Rated voltage	380V	R_r	1.55 Ω
Rated current	6.6A	L_s	0.261 H
Rated frequency	50Hz	L_r	0.261 H
Number of pole pairs	2	M	0.249 H
Rated speed	1430 r/min	J	0.02 kg/m^2
		f	0.0007 Nm.s./rad

Table 1: Induction motor parameters.

The RST controller is made up by the following polynomials:

$$S(z) = (1 - z^{-1})(1 + 0,9989 z^{-1})$$

$$R(z) = 1,4128\text{-}1,4123 z^{-1})$$

$$\mathrm{T(z)} = 4,9974.10^{-4}$$

The stator field oriented control technique is realized with an SVPWM carrier frequency of 16 kHz.

Firstly, a comparison between the performances of the RST versus the classical PID controller is presented in Fig. 1. In this case, the motor currents regulation is made up by conventional PI controllers. The choice of the parameters of speed and currents controllers is done according to the desired performances for the closed loop system by imposing the natural frequency and the damping ratio [17,18]. The reference rotor speed is set at 1000 rpm with a step load torque T_L = 10Nm applied to the system at time t = 1.5 s. It can be seen that the RST controller is better than the classical PID controller in terms of overshoot, settling time and disturbance rejection.

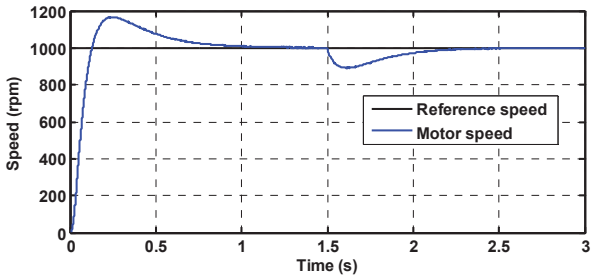

a) Speed time response with conventional PID controller

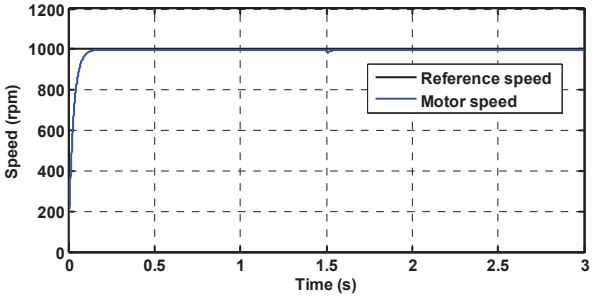

b) Speed time response with RST controller

Fig. 3: Comparison between PID and RST controllers.

The following simulation results are obtained by using the RST controller for speed control and the FOPID controller for currents control as shown in Fig. 1.
Optimization of FOPID controller for currents control needs to define the optimization goals, and then encoding the parameters to be searched. SPEA algorithm runs until the stop criterion is reached. The members of P' in the last generation are the optimized parameters of the FOPID controller. There are five parameters that should be designed according to the control objectives. For FOPID controller, the Crone approximation with order 5 and frequency range equals [1, 1000] rad/s is used. The results of SPEA program for 3 points are given in Table II.

Point	K_p	K_I	K_D	α	β
1	5	400	1	0.84	0.75
2	40	4000	17	0.985	0.865
3	20	2000	5	0.92	0.84

Table 2: FOPID parameters.

Fig. 4 shows the simulation results of speed induction motor control by using the parameters of point 1 of the Table II. A step load torque T_L = 10Nm is applied at time t = 1.5s and removed at time t = 2.5s.

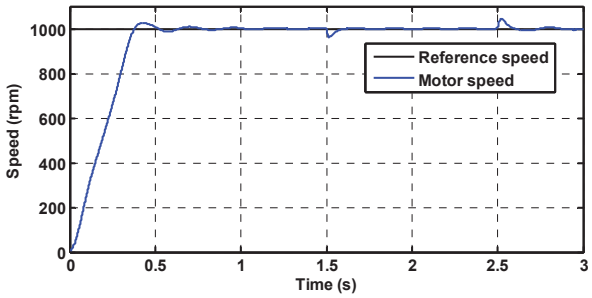

a) Speed time response

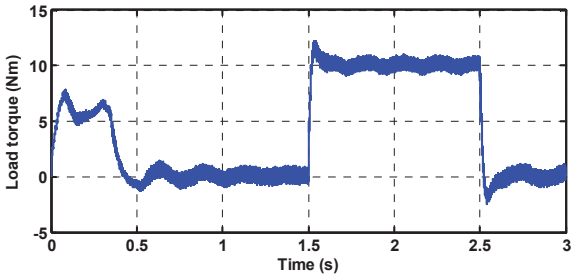

b) Load torque (T_L)

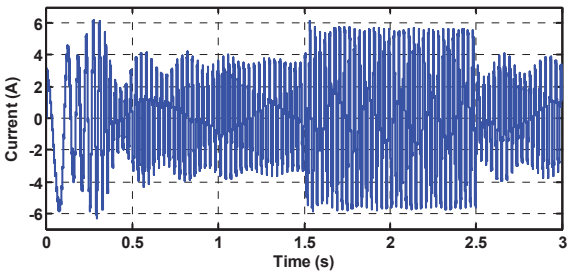

c) Phase current (i_a)

Fig. 4: Simulation results by RST and FOPID controllers with parameters of point 1(Table 2).

Fig.4 shows the overshoot of speed, moreover the engine torque and current ripples. This is due to the FOPID parameters that are not yet optimized (point 1 of FOPID).
The simulation results of Fig. 4 can be improved by using the FOPID parameters of point 2 of Table 2 after first optimization as shown in Fig. 5

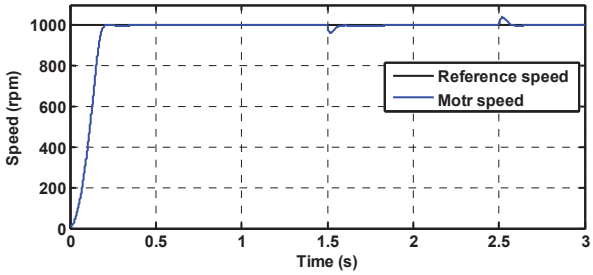

a) Speed time response

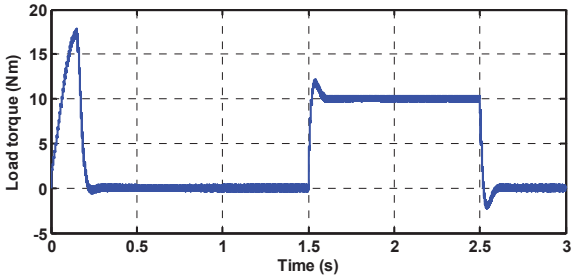

b) Load torque (T_L)

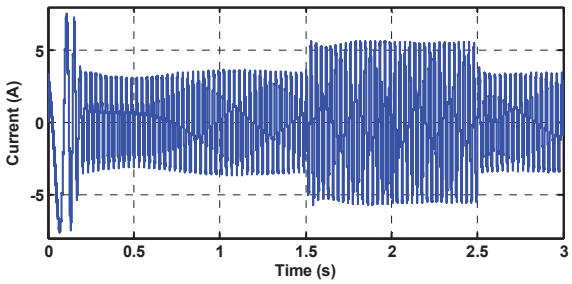

c) Phase current (i_a)

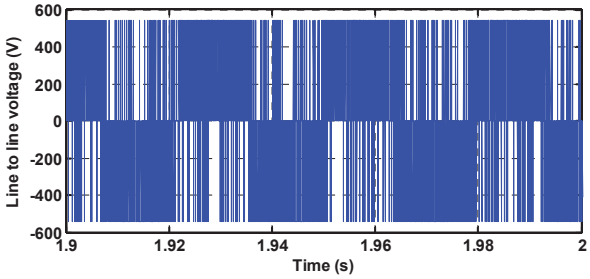

d) Line to line motor voltage (Van-Vbn)

Fig. 5: Simulation results with RST and FOPID controllers with parameters of point 2 (Table 2).

Fig. 5 (d) shows the line to line voltage with unexpected switching that can introduce short circuit in the real systems.

The best simulation results are obtained by using the FOPID with the parameters of the last point of Table II (point 3). In this case, the FOPID controller is well optimazed as shown the simulation results in Fig. 6.

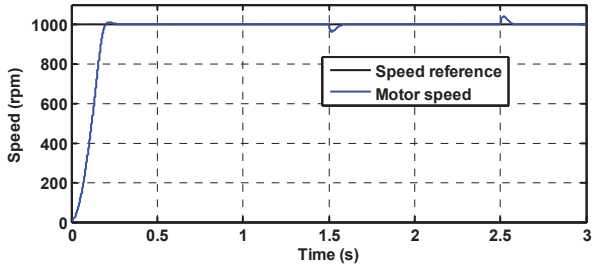

a) Speed time response

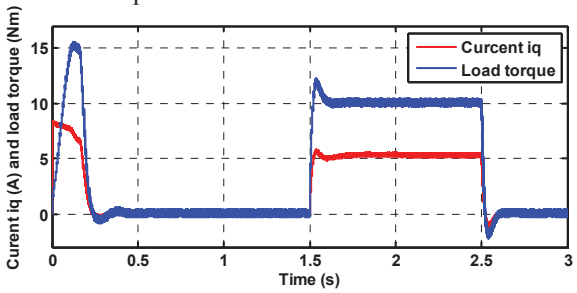

b) q- axis stator current and load torque (i_{qs}, T_L)

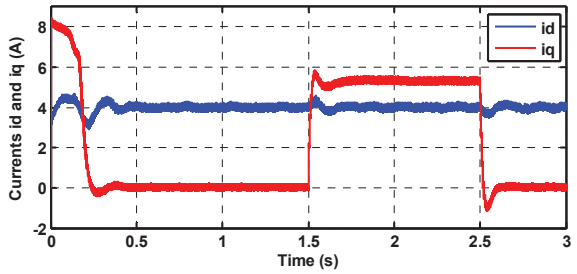

c) d- and q- axis stator currents (i_{ds}, i_{qs})

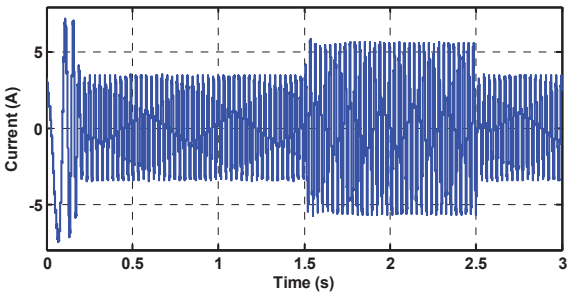

d) Phase current (i_a)

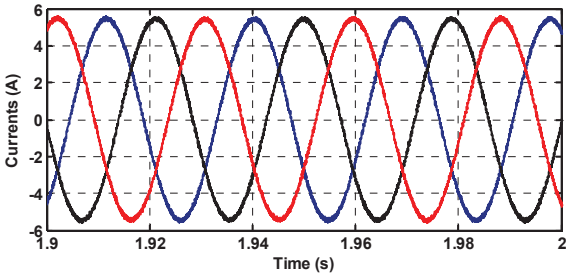

e) Phase currents (i_a, i_b, *and* i_c)

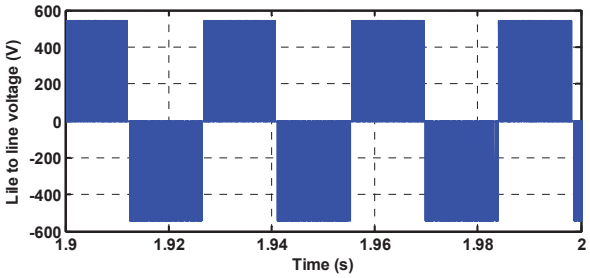

f) Line to line motor voltage (V_{an}-V_{bn})

Fig. 6: Simulation results with RST and FOPID controllers with parameters of point 3 (Table 2).

A robust control of induction motor (Fig. 6) is obtained with the optimized parameters of FOPID controller by using the SPEA algorithm. Both switching peaks at the motor terminals and oscillation on the phase current disappear.

In Fig. 6 (b), it can be seen that the motor torque is proportional to the q-axis stator current i_{qs} as given in (3). Fig. 6 (c) shows that the q-axis current is increased in order to overcome the load torque variation while the d-axis current is maintained at its reference. Fig. 5 (e) show, the stator currents the fixed reference frame (i_a, i_b, i_c). The simulation results show that the RST controller and the ISFOC exhibit good

performances for induction motor drive.

4 Conclusion

In this paper a new robust control system for induction motor drive for EV applications is proposed. High-dynamic performance is obtained using the indirect stator-flux-oriented control (ISFOC) and the space vector pulse width modulation (SVPWM) techniques. An advanced RST controller is designed for speed control loop. This controller can accelerate the response time without overshoot thanks to proper poles placement of the closed loop system. Simulation results show the advantage of the RST controller in comparison to conventional PID controller, in terms of tracking and load torque disturbance rejection.

A fractional order PID controller was designed for motor current regulation loop. This controller has a good dynamic response without unexpected switching behaviour. This controller can resist easily to a disturbance. This makes disturbance rejection tuning independent of the adjustment for speed command tracking. The design of a FOPID requires the use of an algorithm. In this paper SPEA that is a multi-objective optimization approach was used and showed that the tuning of the fractional order PID controller using the proposed method is highly effective.

The simulation results show that the together controllers (RST and FOPID) provide excellent control of induction motor drive used in electric vehicle application.

Nomenclature

v_{ds}, v_{qs}	*d*- and *q*- axis stator voltages.
i_{ds}, i_{qs}	*d*- and *q*- axis stator currents.
Φ_{ds}, Φ_{qs}	*d*- and *q*- axis stator *flux.*
Φ_s	Stator rated flux.
R_s, R_r	Stator and rotor winding resistances.
L_s, L_r, M	Stator, rotor and mutual inductances.
J, f	Rotor inertia and viscous friction coefficient.
N_p	Number of the pole pairs.
ω_s, ω_r, ω_{sl}	Synchronous, rotor and slip angular speed.
Ω, Ω_m	Real and measured mechanical rotor speed.
T_e, T_L	Electromagnetic and load torque.
V_{DC}	Inverter input DC voltage.
τ_s , τ_r	Stator and rotor time constant.
p	Laplace operator.
*	Reference quantities.
T	Sampling period.
ω_0	Natural frequency.
ζ	Damping coefficient.
k	Constant

Acknowledgements

The authors would like to thank Haute-Normandy region and the FEDER for their financial support under VIRTUOSE project.

References

[1] A. Emadi, Y. Joo Lee, K. Rajashekara. “Electronics and motor drives in electric, hybrid Electric, and plug-in hybrid electric vehicles”, *IEEE Trans. Ind. Electron*, **Vol. 55**, no. 6, pp. 2237-2245, (2008).

[2] M. Zeraoulia, M. E. H. Benbouzid and D. Diallo. “Electric motor drive selection issues for HEV propulsion systems: A comparative study”, *IEEE Trans. Veh. Techno*, **Vol. 55**, no. 6, pp. 1756-1764, (2006).

[3] M. B. Camara, H. Gualous, F. Gustin, A. Berthon, B. Dakyo. “DC/DC converter design for supercapacitor and battery power management in hybrid vehicle applications - polynomial control strategy”, *IEEE Trans. Ind. Electron*, **Vol. 57**, no. 2, pp. 587-597, (2010).

[4] A. Tani, M. B. Camara, B. Dakyo, Y. Azzouz. “Embedded energy management based on DC/DC converters - Ultracapacitors and Fuel Cell”, in *proc. ICIT’ 12 Conf.,* pp. 198-204, (2012).

[5] S. Lacroix, M. Hilairet, E. Laboure. “Design of a battery-charger controller for electric vehicle based on RST controller”, in *proc. VPPC*’ 11 *Conf.,* pp. 1-6, (2011).

[6] A. Pintea, D. Popescu, P. Borne. “Robust control for wind power systems”, in *proc. MED’10 Conf.,* pp. 1085-1091, (2010).

[7] M. Bendjedia, Y. Aït-Amirat, B. Walther and A. Berthon. “Digital step motor drive with EKF estimation of speed and rotor position”, *International Review of Electrical Engineering (IREE),* **Vol. 2**, , no. 3, pp. 455 - 465, (2007).

[8] I. Podlubny. “Fractional-order systems and fractional-order controllers”, *Inst. Exp. Phys, Slovak Acad. Sci*.,**Vol. 2**, , no. 2, pp. 28 - 34, (1994).

[9] I. Podlubny. “Fractional-order systems and $PI^{\lambda}D^{\mu}$-controllers”, *IEEE Trans. Trans. on Automatic Control*, **Vol. 44**, no. 1, pp. 208-214, (1999).

[9] L. Meng, D. Xue. “Design of an optimal fractional-order PID controller using multi-Objective GA optimization”, in *proc. CCDC’09 Conf.,* pp. 3849-3853, (2009).

[10] B. T. Zhang, Y. Pi. “Robust fractional order proportion-plus-differential controller based on fuzzy inference for permanent magnet synchronous motor”, *IET,* **Vol. 6**, no. 6, pp. 829-837, (2012).

[11] Y. Zhao, Y. Gao, Z. Hu, Y. Yang, J. Zhan, Y. Zhang. “Damping Inter Area Oscillations of Power Systems by a Fractional Order PID Controller”, in *proc. Energy and Environment Technology Conf.,* pp. 103-106, (2009).

[12] J. Y. Cao and B. G. Cao. “Design of fractional order controller based on particle swarm optimization”, *Journal of Control, Automation, and Systems*, **Vol. 4**, no. 6, pp. 775-781, (2006).

[13] D. Kundu, K. Suresh, S. Ghosh and S. Das. “Designing fractional-order PID controller using a modified invasive weed optimization algorithm”, *World Congress on Nature and Biologically Inspired Computing,* pp. 1315-1320, (2009).

[14] M. Cai, X. Pan, Y. Du. “New elite multiparent crossover evolutionary optimization algorithm of parameters

tuning of fractional-order PID controller and its application", in *pro.Innovative Computing, Information and Control,* pp. 64-67, (2009).

[15] E .Zitzler, and L. Thiele. "Multi-objective evolutionary algorithms: A comparative case study and the Strength Pareto approach", *IEEE Trans.* Evolutionary computation, **Vol. 3**, no. 4, pp. 257-271, (1999).

[16] A. K. Tehrani, A. Rafei, S. M. R. Griva, L. Brandon, M. Hamzaoui, I. Rasoanarivo, and F. M. Sargos. "Design of fractional order PID controller for boost converter on multi-objective optimization", *in proc. EPE-PEMC'10*, pp. T3. 179-185, (2009).

[17] Y. Agrebi, M. Triki,Y. Koubaa et M. Boussak. "Rotor speed estimation for indirect stator flux oriented induction motor drive based on MRAS scheme", *Journal of Electrical Systems*, **Vol. 3**, no. 3, pp. 131-143, (2007).

[18] M. Boussak, K. Jarray. "A high-performance sensorless indirect stator flux orientation control of induction motor drive", *IEEE Trans. Ind. Electron*., **vol. 53**, no. 1, pp. 41–49, (2006).

[19] A. Iqbal, and S. Moinuddin. "Comprehensive relationship between carrier-based PWM and space vector PWM in a five-phase VSI", *IEEE Trans. Power Electron.* , **vol. 24**, no. 10, pp. 2379-2390, (2009).